AAPPS Bulletin

REVIEW ARTICLE

Open Access

β-Ga_2O_3 material properties, growth technologies, and devices: a review

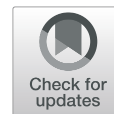

Masataka Higashiwaki

Abstract

Rapid progress in β-gallium oxide (β-Ga_2O_3) material and device technologies has been made in this decade, and its superior material properties based on the very large bandgap of over 4.5 eV have been attracting much attention. β-Ga_2O_3 appears particularly promising for power switching device applications because of its extremely large breakdown electric field and availability of large-diameter, high-quality wafers manufactured from melt-grown bulk single crystals. In this review, after introducing material properties of β-Ga_2O_3 that are important for electronic devices, current status of bulk melt growth, epitaxial thin-film growth, and device processing technologies are introduced. Then, state-of-the-art β-Ga_2O_3 Schottky barrier diodes and field-effect transistors are discussed, mainly focusing on development results of the author's group.

Keywords: Gallium oxide (Ga_2O_3)

1 Introduction

There is no room for doubt that silicon (Si) has been the fundamental material serving as the backbone technology of semiconductor device electronics. Generally speaking, up to now, the vast majority of electronic systems are based on Si devices such as metal-oxide-semiconductor field-effect transistors (MOSFETs), bipolar transistors, and some types of diodes. Their performance has tremendously improved by means of uninterrupted innovation in its material and device processing technologies for over the last 70 years. However, performance of Si devices has almost reached the fundamental upper limit expected from its material properties, and it is difficult to keep improving the performance at the same pace as before. In this current situation, research and development (R&D) of FETs and diodes exploiting new semiconductors, which have better physical properties for specific applications than those of Si, has been getting more active from expectations that they may open up a new field of semiconductor electronics and/or elicit characteristics that far exceed those of Si devices. Most of semiconductor physical properties are determined by their bandgap; therefore, bandgap engineering has been one of the main directions for exploring new materials, and a new semiconductor should have a different bandgap energy (E_g) from that of any existing material. Among a variety of new materials, wide bandgap (WBG) semiconductors are expected to be promising for power switching applications, since the WBG devices can offer advantages of high efficiency and power density over Si devices. The two most promising WBG semiconductors are silicon carbide (SiC) and gallium nitride (GaN); their FETs and diodes have already penetrated into the market.

Recently, a new category called "ultrawide bandgap (UWBG) semiconductor" has attracted great attention due to their strong potential providing new and exciting research opportunities for various applications, and R&D on UWBG materials and devices continues to expand over the years [1]. The UWBG semiconductors are defined by E_g exceeding those of SiC (3.3 eV) and GaN (3.4 eV). High Al-content AlGaN, diamond, and cubic boron nitride are included in the UWBG materials. A new semiconductor gallium oxide (Ga_2O_3), which is the main topic of this

Correspondence: mhigashi@nict.go.jp
Green ICT Device Laboratory, Koganei Frontier Research Center, Advanced ICT Research Institute, National Institute of Information and Communications Technology, 4–2–1 Nukui-Kitamachi, Koganei, Tokyo 184-8795, Japan

© The Author(s). 2022 **Open Access** This article is licensed under a Creative Commons Attribution 4.0 International License, which permits use, sharing, adaptation, distribution and reproduction in any medium or format, as long as you give appropriate credit to the original author(s) and the source, provide a link to the Creative Commons licence, and indicate if changes were made. The images or other third party material in this article are included in the article's Creative Commons licence, unless indicated otherwise in a credit line to the material. If material is not included in the article's Creative Commons licence and your intended use is not permitted by statutory regulation or exceeds the permitted use, you will need to obtain permission directly from the copyright holder. To view a copy of this licence, visit http://creativecommons.org/licenses/by/4.0/.

article, is a key material among the UWBG semiconductors. Ga_2O_3 can offer two fundamental advantages over SiC and GaN: a very large E_g and ease of bulk wafer production.

Ga_2O_3 is by no means a novel material; it has a long R&D history for over 70 years [2]. However, Ga_2O_3 had been largely ignored by a majority of semiconductor researchers and engineers, which resulted in it falling behind SiC and GaN. The achievement of the first single-crystal Ga_2O_3 FET in 2011 is widely credited with changing the situation and invigorating Ga_2O_3 R&D [3]. As shown in Fig. 1, the number of publications on Ga_2O_3 significantly increases in recent years according to increased recognition among semiconductor researchers and engineers that Ga_2O_3 has unique and attractive material properties for various optoelectronics applications.

This article provides a comprehensive review on current β-Ga_2O_3 material and device technologies. It should be noted that although several polymorphs exist for Ga_2O_3 as introduced in Section 2.1, discussions in this review will just focus on β-Ga_2O_3. Following this introduction in Section 1, Section 2 describes basic physical properties of β-Ga_2O_3. Sections 3 and 4 provide melt bulk and epitaxial thin-film growth technologies for β-Ga_2O_3, respectively. Selected elemental device processing technologies are given in Section 5. Development history of β-Ga_2O_3 Schottky barrier diodes (SBDs) and FETs in the author's group are introduced in Sections 6 and 7, respectively, together with representative achievements reported from other institutes. Section 8 concludes this article.

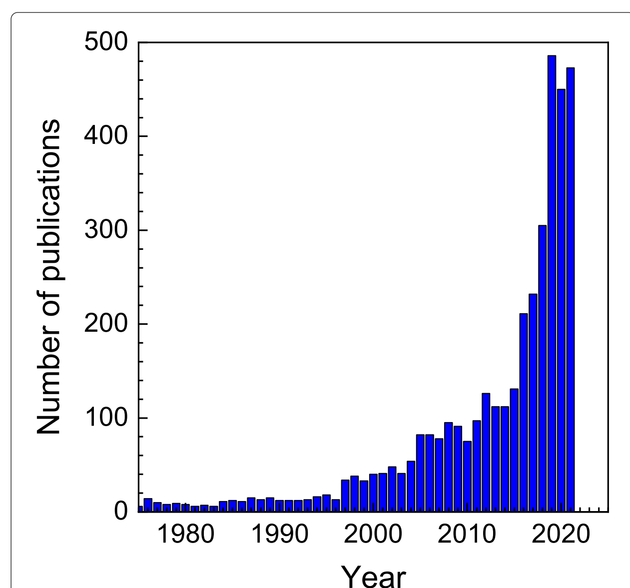

Fig. 1 Number of publications on Ga_2O_3 from 1975 to 2020. The papers were searched with criterion of containing "Ga_2O_3" in the title (data: Web of Science as of November 30, 2021)

2 Physical properties

The important material parameters of β-Ga_2O_3 for electronic device applications are listed in Table 1, together with those of Si, SiC, and GaN. The material parameters and the other important features are discussed in this section.

2.1 Polymorph

Five types of Ga_2O_3 polymorphs denoted by α, β, γ, δ, and ϵ were first reported in 1952 [2]. The β phase is a thermodynamically stable form, and the others are metastable. β-Ga_2O_3 has the β-gallia monoclinic structure with lattice constants of 12.2, 3.0, and 5.8 Å in the *a*, *b*, and *c* axes, respectively, and the angle between the *a* and *c* axes is about 104° [4]. A schematic of the β-Ga_2O_3 unit cell is depicted in Fig. 2. The β-Ga_2O_3 crystal structure is composed of two inequivalent Ga sites and three inequivalent O sites. Ga(I) and Ga(II) are tetrahedrally and octahedrally coordinated with O, respectively. O(I) and O(II) have threefold Ga coordination, while O(III) has fourfold. The important feature of β-Ga_2O_3 in contrast to the other polymorphs is that bulk single crystals can be synthesized by melt growth methods; the details will be given in Section 3.

2.2 Band structure

β-Ga_2O_3 has an isotropic and dispersive conduction band minimum comprised of the Ga 4*s* states, and an anisotropic and fairly flat valence band maximum made up of the O 2*p* states with contributions of the Ga 3*d* and 4*s* orbitals [5–7]. These band structures provide sufficient electron conduction associated with a reasonable electron effective mass of $\sim 0.3m_0$ (m_0: free electron mass)

Table 1 Comparisons of material properties between major semiconductors and β-Ga_2O_3

	Si	4H-SiC	GaN	β-Ga_2O_3
Bandgap E_g (eV)	1.1	3.3	3.4	4.5
Relative dielectric constant ϵ	11.8	9.7	9.0	10.2–12.4
Breakdown electric field E_{br} (MV/cm)	0.3	2.5	3.3	> 7
Room-temperature electron mobility μ (cm^2/Vs)	1400	1000	1200	$\sim$200
Saturation electron velocity V_{sat} ($\times 10^7$ cm/s)	1.0	2.0	2.5	1.0–1.5
Thermal conductivity (W/cmK)	1.5	2.7	2.1	0.11–0.27
Baliga's figure of merit ($= \epsilon \mu {E_{br}}^3$)	1	340	870	1570–1900
Johnson's figure of merit ($= {E_{br}}^2 {V_{sat}}^2$)	1	280	760	540–1200

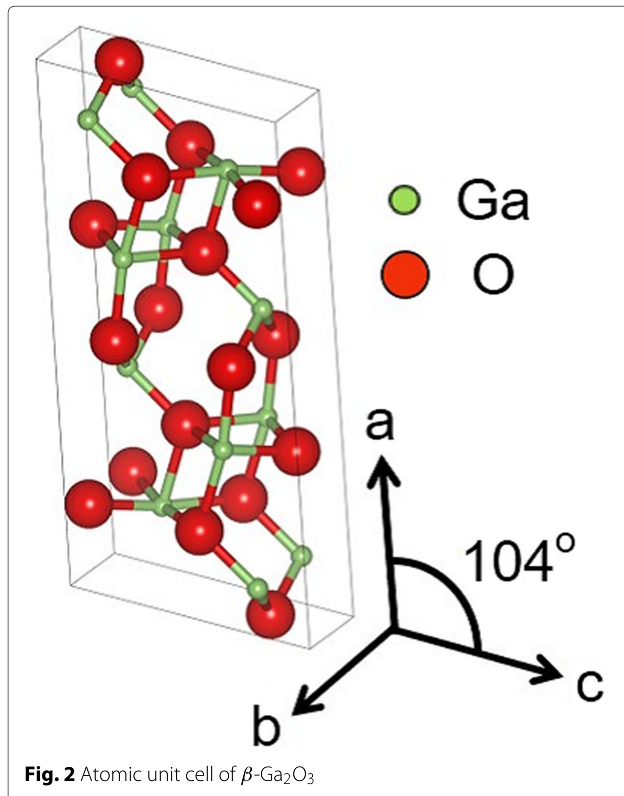

Fig. 2 Atomic unit cell of β-Ga_2O_3

[5–8] and limited hole conduction due to three factors described in Section 2.6.2.

First-principles calculations based on hybrid density functional theory predicted an E_g of 4.6–4.9 eV for β-Ga_2O_3 [5–7]. For a long term, there has also been intense discussion on whether β-Ga_2O_3 is a direct or an indirect semiconductor. As an answer to this scientific question, Onuma et al. reported that energies of absorption edges in β-Ga_2O_3 melt-grown bulk single crystals can be divided into six ranges within 4.4-5.3 eV according to the selection rules of optical transition caused by the anisotropic valence band maximum and that the direct and indirect E_g were estimated to be 4.48 and 4.43 eV, respectively [9]. In other words, these experimental results indicate that the energy difference between the direct and indirect E_g of β-Ga_2O_3 is negligibly small at room temperature.

2.3 Breakdown electric field

The breakdown electric field (E_{br}) is an intrinsic property that each material has and corresponds to the maximum electric field that the material structure can support before avalanche breakdown. The larger E_{br} leads to greater voltage blocking capability of devices, that is, a larger breakdown voltage (V_{br}). Theoretical calculation predicted that β-Ga_2O_3 possesses an extremely large E_{br} of over 8 MV/cm [10]. However, in fact, the breakdown events for all of the Ga_2O_3 FETs and diodes reported so far were caused by their permanent failure due to electric field concentration at a gate or an anode electrode edge; therefore, the intrinsic E_{br} of β-Ga_2O_3 in terms of the avalanche breakdown has never been observed. For reference, the maximum E_{br} experimentally derived from structural failure of a high-k dielectric/n-Ga_2O_3 diode was ~7 MV/cm [11].

2.4 Electron mobility

The primitive cell of β-Ga_2O_3 gives rise to many phonon modes due to a lack of symmetry for its monoclinic structure. Among the various modes, the longitudinal optical (LO) phonon with energies of 20–40 meV has the highest impact on low-field electron mobility (μ) in β-Ga_2O_3 bulks [12]. This is the main factor why the room temperature μ of n-Ga_2O_3 is theoretically expected to be limited up to ~200 cm^2/Vs [13, 14], even though the electron effective mass is comparable to those of the other WBG semiconductors. Actually, the peak room temperature and low temperature μ of n-Ga_2O_3 films experimentally measured were 150–180 and 5000–10,000 cm^2/Vs, respectively [15–18].

2.5 Saturation electron velocity

The high-field carrier transport is another important factor having a large impact on electronic device performance. The saturation electron velocity (v_{sat}) in β-Ga_2O_3 was theoretically predicted to be 1–2×10^7 cm/s [19], which is equivalent to that in Si and about half of those in SiC and GaN. It should be noted that the v_{sat} is sufficiently good for many of high-frequency applications.

2.6 Doping

2.6.1 n-type

Si, germanium (Ge), and tin (Sn) are often used as donor dopants for β-Ga_2O_3. These group IV elements form shallow donor states in Ga_2O_3 [20, 21], and their activation ratios at room temperature are very high (~100% for Si). The electron density (n) in β-Ga_2O_3 can be precisely controlled in a wide range of 10^{15}–10^{20} cm^{-3} by using the donor dopants. As for controllability of n-type conductivity, Ga_2O_3 is absolutely the same as other semiconductors.

2.6.2 p-type

Contrary to the ease of n-type doping, a major drawback of Ga_2O_3 has been a lack of hole-conductive p-type material, which is the most serious limitation for development of Ga_2O_3 devices. In fact, there has been no report on successful p-type doping with effective hole conduction, even though there are some potential acceptor dopants: magnesium (Mg), zinc (Zn), and beryllium (Be) as cation substituting dopants and nitrogen (N) as an anion substituting one. There are three factors to make it almost impossible to realize hole-conductive p-type Ga_2O_3. First, it is generally difficult for single-crystal oxide semiconductors

to form shallow acceptor states, since their valence band states are mainly composed of the weakly interacting O 2*p* orbitals as discussed in Section 2.2. Theoretical calculations predicted that all the acceptor candidates would exhibit extremely large activation energies of over 1 eV [22, 23]. Another expected factor limiting hole conductivity is the very low μ and diffusion constant owing to the heavy hole effective mass originated from the flat valence band maximum [5–7]. Furthermore, it was also theoretically predicted that holes localize in β-Ga_2O_3 as small polarons due to lattice distortion, as opposed to being free holes widely populating [24–26]. From the three factors, hole-conductive *p*-Ga_2O_3 seems to be hardly realized. However, *p*-Ga_2O_3 layers formed by the deep-acceptor doping are useful to form a large energy barrier of over 3 eV in *n*-Ga_2O_3 by utilizing the built-in potential at the *p*-*n* junction.

2.7 Thermal conductivity

The thermal conductivity is one of the important parameters to make a great impact on performance of high-power devices, since it limits dissipation capacity of heat generated by on-state conduction loss in the channel and/or drift regions. Ga_2O_3 has a significantly lower thermal conductivity compared to those of the other power semiconductors as listed in Table 1 [27–30]. The thermal conductivity of β-Ga_2O_3 is anisotropic due to the monoclinic lattice structure; they were estimated to be 0.22–0.27 W/cmK in the [010] direction (highest) and 0.11–0.14 W/cmK in the [100] direction (lowest). The low thermal conductivity will not only hamper high-power device performance but also limit long-term device reliability. Hence, thermal management is one of the key technical challenges for future practical applications and industrialization of Ga_2O_3 RF and power devices.

2.8 Device figure of merit

There are several device figures of merit (FOMs) to estimate how suitable a semiconductor material is for specific device application. Here, two FOMs are discussed: Baliga's FOM (BFOM) [31, 32] and Johnson's FOM (JFOM) [33].

BFOM is commonly used as a parameter to estimate potential of semiconductor materials for power switching device applications. The BFOM of β-Ga_2O_3 is several times larger than those of SiC and GaN. This is because BFOM is proportional to the cube of E_{br} but only linearly proportional to μ. Therefore, we can expect from the BFOM that β-Ga_2O_3 power devices can offer lower conduction loss compared with the other semiconductor devices listed in Table 1 when designing the structure for a given voltage.

We use JFOM to estimate material potential for RF power FET applications. The JFOM of β-Ga_2O_3 is estimated to be the same level as or a little inferior to that of GaN. However, the actual power efficiency of FETs used in RF amplifiers is generally $\sim$50%, that is, the other half loss converts to heat. Thus, it is expected that the poor heat dissipation capacity of β-Ga_2O_3 attributed to its low thermal conductivity becomes much more serious for applications to RF devices rather than power switching devices.

3 Melt bulk growth

The availability of affordable native wafers manufactured from melt-grown bulk single crystals is one of the distinctive features for β-Ga_2O_3 and offers a significant advantage of Ga_2O_3 over SiC and GaN in terms of wafer size, crystal quality, and production cost, because SiC and GaN bulk crystals require alternative synthesis techniques using higher pressure and temperature. β-Ga_2O_3 bulk single crystals have been synthesized by various melt growth methods illustrated in Fig. 3, such as floating zone [34, 35], Czochralski (CZ) [36, 37], vertical Bridgman [38], and edge-defined film-fed growth (EFG) [35, 39]. Si or Sn is usually used as a donor dopant to control *n*, and semi-insulating Ga_2O_3 bulks are producible through compensation of residual donors with Fe or Mg doping. Now, *n*-type and semi-insulating β-Ga_2O_3 wafers manufactured from CZ and EFG bulks are made commercially available to the public, which are of sufficiently high quality for development of various Ga_2O_3 devices.

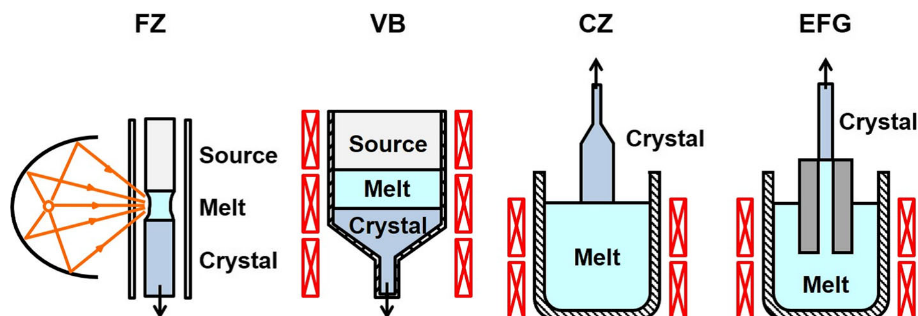

Fig. 3 Melt growth methods for synthesis of β-Ga_2O_3 bulk single crystals

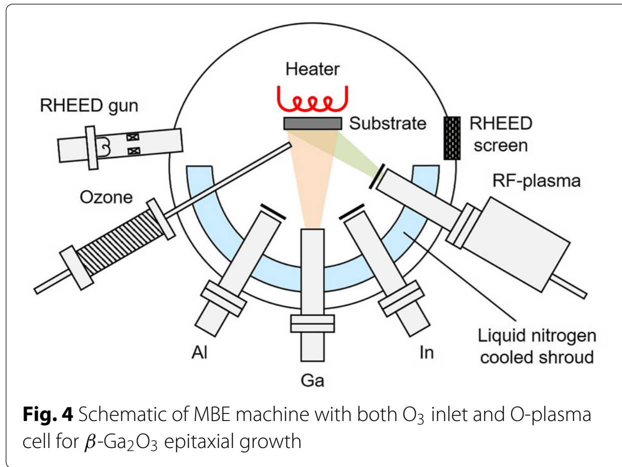

Fig. 4 Schematic of MBE machine with both O_3 inlet and O-plasma cell for β-Ga_2O_3 epitaxial growth

4 Epitaxial growth

4.1 Molecular beam epitaxy

Molecular beam epitaxy (MBE) is an epitaxial growth technique conducted in ultrahigh vacuum and enables precise control of layer thickness. As other compound semiconductors, MBE has been the most commonly used for thin-film growth of Ga_2O_3 in the early days of R&D. Figure 4 depicts a schematic of a typical MBE machine for Ga_2O_3 growth. An effusion cell is used to sublimate a Ga metal source in order to form molecular beam flux that travels in a line of sight toward a substrate. Ga_2O_3 epitaxial growth happens on the substrate by means of oxidization of supplied Ga atoms using oxidant such as ozone (O_3) and oxygen (O) radicals. Two-step reaction happens between Ga and O during Ga_2O_3 MBE growth [40]. In the first stage of growth, volatile gallium suboxides (Ga_2O) are formed by oxidization of supplied Ga atoms on the growth surface. Then, in the second stage, Ga_2O desorbs from the growth surface or is incorporated into a Ga_2O_3 epitaxial layer by becoming Ga_2O_3 through a further oxidization process. Due to this unique growth kinetics, the growth rate strongly depends on growth parameters such as O/Ga flux ratio, growth temperature, and substrate orientation, since it is determined by competition between the Ga_2O desorption and oxidization processes. Intentional n-type doping has been demonstrated by using Si, Sn, and Ge as donor dopants [41–44]. However, it is difficult to control a low doping density on the order of 10^{16} cm^{-3} or less, because the surface of the dopant source in an effusion cell is easily oxidized during the MBE growth by background O species, resulting in the dopant flux hardly controlled. Furthermore, there is a specific issue only for Sn atoms that they tend to segregate on the growth surface without being incorporated into the epitaxial film [45]. At present, MBE-grown β-Ga_2O_3 epitaxial wafers are mainly utilized for fabrication of lateral FETs, and both of the MBE methods using O_3 and O radicals can provide high-quality β-Ga_2O_3 films sufficient for the device development.

4.2 Halide vapor phase epitaxy

High-speed β-Ga_2O_3 thin-film growth attained by halide vapor phase epitaxy (HVPE) was first reported in 2014 [46]. The crystal quality of the HVPE-grown β-Ga_2O_3 films was excellent from the beginning. Figure 5 illustrates a schematic of an HVPE reactor for Ga_2O_3 growth. Gallium monochloride (GaCl) and O_2 are typically used as Ga and O precursors, respectively. The growth rate of β-Ga_2O_3 thin films can be increased up to 20 μm/h without any degradation of crystal quality. The background n of unintentionally doped (UID) β-Ga_2O_3 (001) films is very low, which is less than 1×10^{13} cm^{-3} [47]. Si doping performed by simultaneous supply of $SiCl_4$ during the Ga_2O_3 growth can provide accurate control of n in a wide range from 10^{15} to 10^{19} cm^{-3} [15]. The maximum electron μ in HVPE-grown Si-doped n-Ga_2O_3 films is $\sim$150 cm^2/Vs at room temperature reported so far [15]. In recent years, epitaxial wafers with HVPE-grown n-Ga_2O_3 layers are mass produced and widely utilized for development of vertical FETs and SBDs around the world.

4.3 Metalorganic chemical vapor deposition

Metalorganic chemical vapor deposition (MOCVD) is a well-established epitaxial growth technique for compound semiconductors and is often employed for

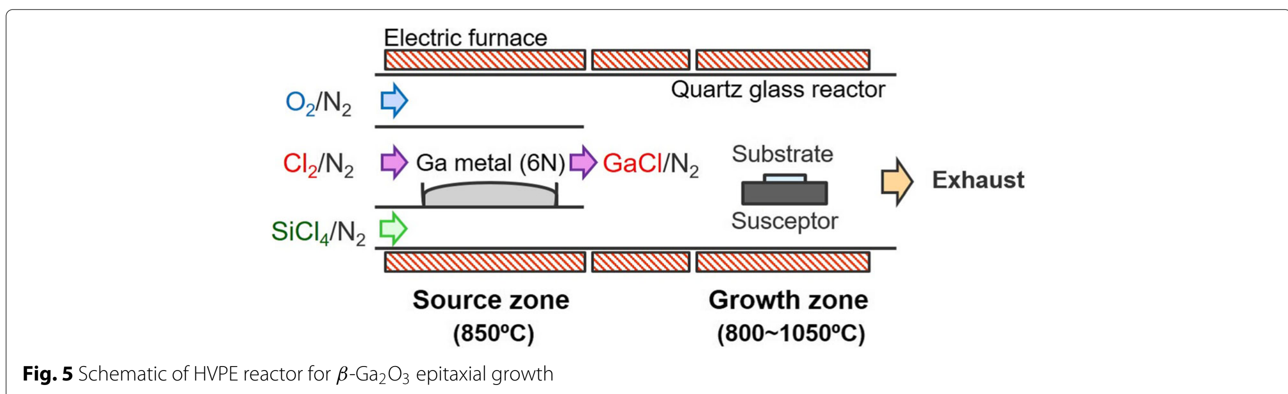

Fig. 5 Schematic of HVPE reactor for β-Ga_2O_3 epitaxial growth

production of high-quality epitaxial wafers on an industrial scale. There used to be some limitations for Ga_2O_3 MOCVD growth, such as low growth rate, high-density background n, and low electron μ. However, most of the technical issues have been resolved within the last 5 years, and MOCVD can provide high-quality β-Ga_2O_3 films required for device development now. In a Ga_2O_3 MOCVD reactor as shown in Fig. 6, traditional Ga precursors such as trimethylgallium (TMGa) and triethylgallium (TEGa), and high-purity O_2 and H_2O are generally used for the growth. Si donor doping can be done by simultaneous supply of Si-containing precursors.

The growth rate has been increased to ~4 μm/h through optimization of growth condition [48]. The background n of MOCVD-grown UID β-Ga_2O_3 films is now at a low level of less than 1×10^{16} cm^{-3} [17, 49]. The peak electron μ of Si-doped n-Ga_2O_3 films were ~180 and ~10,000 cm^2/Vs at room temperature and 45 K, respectively [16–18]. These electrical properties are comparable with those of HVPE-grown films. Furthermore, MOCVD can offer high-quality β-$(AlGa)_2O_3$ thin films and β-$(AlGa)_2O_3$/Ga_2O_3 heterostructures [50, 51]; this is an important advantage of MOCVD over HVPE.

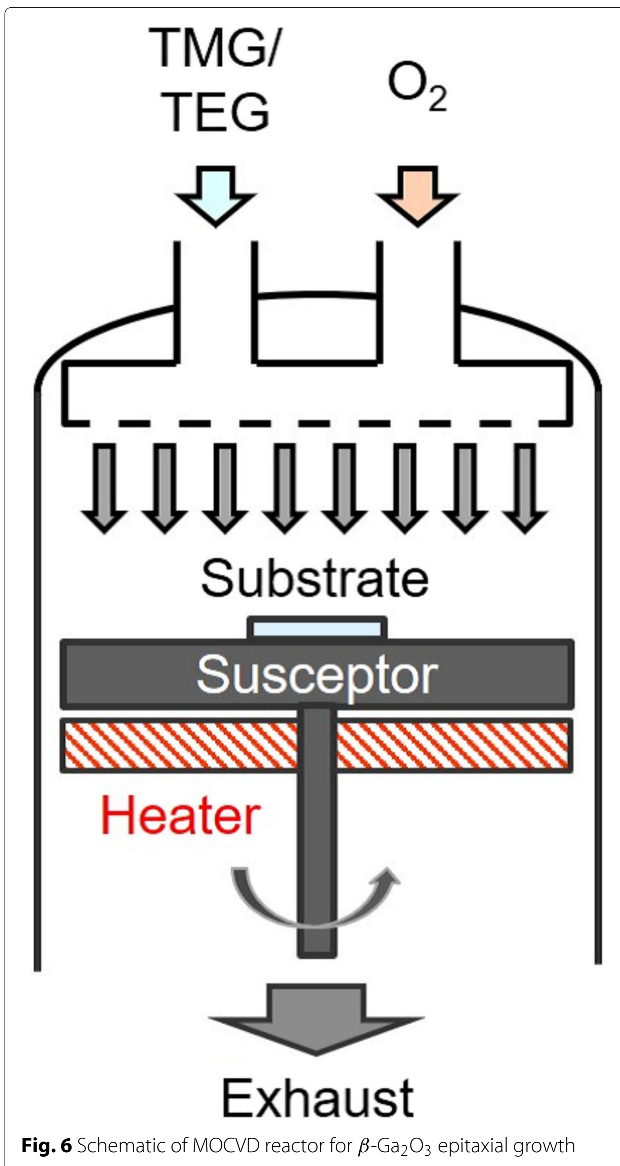

Fig. 6 Schematic of MOCVD reactor for β-Ga_2O_3 epitaxial growth

5 Device process technologies

5.1 Ion implantation doping

For β-Ga_2O_3, ease of ion implantation doping has gained less attention compared with other features; however, this is definitely important for mass production of β-Ga_2O_3 devices in the future. Here, ion implantation doping processes developed for β-Ga_2O_3 by the author's group are presented.

5.1.1 n-type

Si-ion implantation doping process was developed to fabricate ohmic electrodes on n-Ga_2O_3 [52]. Implanted Si atoms start to be activated by annealing at 800°C, and the activation ratio becomes the highest at 900–1000°C. Note that the activation ratio also depends on the Si doping density. The highest n of Si-doped β-Ga_2O_3 layers formed by implantation was 3×10^{19} cm^{-3} for a Si density of 5×10^{19} cm^{-3}, which is high enough to form decent ohmic electrodes with a low contact resistance. The typical room-temperature electron μ of n-Ga_2O_3 layers with an n of low- to mid-10^{17} cm^{-3} formed by Si-ion implantation is ~100 cm^2/Vs [53], which is comparable with those of n-Ga_2O_3 layers prepared by in-situ donor doping during epitaxial growth. The Si-ion implantation doping is useful for formation of not only ohmic electrodes but also FET channels; the author's group has been using this technique to form n-Ga_2O_3 active regions in various types of devices.

5.1.2 Deep acceptor p-type

The author's group attempted to develop ion implantation doping processes for deep acceptor species to form a large energy barrier in n-Ga_2O_3 provided by the built-in potential of the p-n junction rather than a hole-conductive p-Ga_2O_3 layer. We first tried Mg as a deep-acceptor candidate, because it is predicted to be the most stable cation-site acceptor with the lowest formation energy in β-Ga_2O_3 [22, 23]. Mg-ion implantation doping into n-Ga_2O_3 bulk crystals and subsequent annealing converts the n-type conductivity into semi-insulating, which is attributed to compensation of the donors by the doped Mg [54]. However, implanted Mg atoms significantly diffuse during the activation annealing; in consequence, it is difficult to precisely control their depth profile.

We chose N as an alternative candidate of deep acceptor for β-Ga_2O_3. N is the closest to O in terms of ionic size

and electronic structure and thus can be expected to be the most possible anion-substituting acceptor. Implanted N atoms in n-Ga_2O_3 effectively activate by annealing at temperatures of higher than 1100°C and contribute to compensation of the background donors [54]. Furthermore, the N atoms exhibit much lower diffusivity in β-Ga_2O_3 than Mg atoms, which helps to keep the doping profile even after high-temperature activation annealing.

Test structures with a Mg- or a N-doped current blocking layer (CBL) as shown in Fig. 7a were fabricated by ion implantation processes to compare their leakage characteristics. The N-doped structure provided much lower leakage current compared with the Mg-doped one [Fig. 7b], because the N profile was maintained even after activation annealing due to its less diffusivity. These results indicate that N-ion implantation is more useful for device fabrication than Mg-ion implantation.

5.2 Metal/n-Ga_2O_3 contacts

5.2.1 Schottky contact

A variety of Schottky metals including tungsten (W), copper (Cu), nickel (Ni), iridium (Ir), platinum (Pt), and gold (Au) have been reported for n-Ga_2O_3 [55–57]. Pt and Ni are the most common ones used for device fabrication among them. The Schottky contacts on n-Ga_2O_3 are usually of high quality, which is typified by an ideality factor close to unity. The barrier height between the metal and n-Ga_2O_3 reported so far is 1.0–1.5 eV, depending on the metal species and the crystal orientation of β-Ga_2O_3 surface. Layered oxide metal $PdCoO_2$ also forms a high-quality Schottky junction with n-Ga_2O_3 [58].

5.2.2 Ohmic contact

Titanium (Ti)-based metal stacks typified by Ti/Au have been commonly used to fabricate ohmic electrodes on n-Ga_2O_3. It should be noted that Ti-based electrodes formed on n-Ga_2O_3 can provide ohmic characteristics only in case of $n > 10^{18}$ cm^{-3}; therefore, formation of n^+-Ga_2O_3 is absolutely necessary to fabricate ohmic contacts. Si-ion implantation doping and regrowth have been utilized to form n^+-Ga_2O_3 ohmic regions [52, 59, 60]. The post-metallization annealing provides short-range intermixing of Ti and Ga_2O_3 at the interface, resulting in further reduction in contact resistance and improvement in reliability and endurance [61–63]. The routine process developed in the author's group based on the Si-ion implantation doping described in Section 5.1.1 and post-metallization annealing can provide a low specific contact resistance of less than 1×10^{-5} Ωcm^2. Transparent amorphous oxides such as indium tin oxide and zinc oxide have also been tested as ohmic electrodes [64–66].

5.3 Etching

Dry etching processes such as BCl_3-based reactive-ion etching (RIE) and inductively coupled plasma RIE (ICP-RIE) are most commonly used for fabrication of β-Ga_2O_3 devices [67, 68]. It is also possible to perform wet etching of β-Ga_2O_3 using hot acid such as H_3PO_4 and H_2SO_4 [69, 70]. Dry etching often causes plasma damage on the Ga_2O_3 surface [71], and wet etching is effective to remove the damaged region [72]. Metal-assisted chemical etching, which is a technique to use Pt having a catalytic effect as an etching mask, is unique and useful to fabricate mesa structures and fin arrays with a high aspect ratio [73].

5.4 Direct wafer bonding

The performance of many types of semiconductor devices is limited by their heat dissipation capacity, since heat generation under high-power operation is inevitable even for high-efficiency power devices, and an electrical resistance of the drift layer increases with rising operation temperature due to a decrease in electron

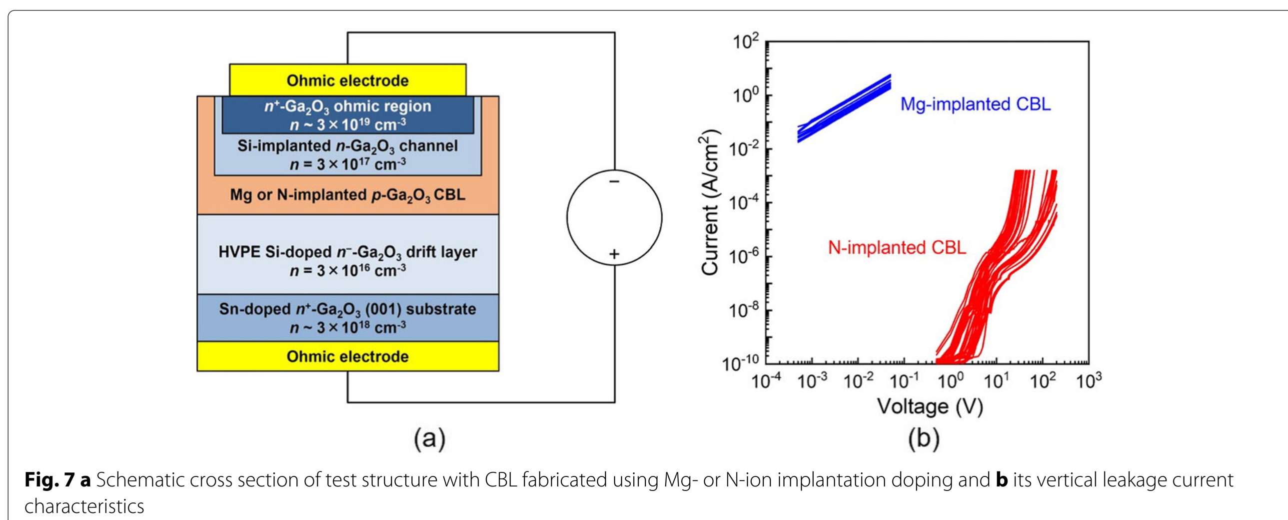

Fig. 7 a Schematic cross section of test structure with CBL fabricated using Mg- or N-ion implantation doping and **b** its vertical leakage current characteristics

μ. Therefore, for Ga_2O_3 device technologies, the low thermal conductivity is a serious potential weakness, and thermal management is one of the most important R&D challenges. One of the effective ways to improve heat dissipation from Ga_2O_3 devices is heterogeneous integration of Ga_2O_3 active layers with foreign substrates having high thermal conductivity such as SiC and diamond by direct bonding [74–77]. The author's group performed surface activated bonding between single-crystal β-Ga_2O_3 and cost-effective polycrystalline SiC substrates. The Ga_2O_3/SiC bonded substrate demonstrated superior characteristics such as a large mechanical bonding strength of over 10 MPa, a small specific electrical resistance of 2×10^{-4} Ωcm^2, and a negligibly small thermal resistance at the bonding interface [74].

6 SBD

WBG- and UWBG-semiconductor SBDs can offer some advantages against Si diodes mainly based on their large BFOMs: higher V_{br}, lower on-resistance (R_{on}), higher efficiency, and faster switching speed. A variety of Ga_2O_3 SBDs have been developed over the last decade. Primitive Ga_2O_3 SBDs were fabricated with a β-Ga_2O_3 bulk wafer synthesized by EFG [78]. At the time, β-Ga_2O_3 epitaxial wafers with a thick drift layer having $n < 10^{17}$ cm^{-3} were hardly available, since MBE was the only technique that could provide high-purity epitaxial layers but was not able to provide n-Ga_2O_3 layers with a low n satisfying requirement for fabrication of high-voltage devices due to technical limitation of donor doping [45]. The HVPE technology became a breakthrough for the development of vertical β-Ga_2O_3 devices, because high-quality, low-doped n-Ga_2O_3 drift layers were made available thanks to it. Simple β-Ga_2O_3 SBDs with HVPE-grown drift layers demonstrated excellent current–voltage output characteristics following the thermionic emission and thermionic field emission models at forward- and reverse-bias conditions, respectively [79], which are typical behaviors for WBG and UWBG semiconductors. The next step was enhancement of V_{br} to prove that β-Ga_2O_3 SBDs are useful for high-voltage applications. First demonstration of Ga_2O_3 SBDs with $V_{br} > 1$ kV was achieved by applying a field plate to mitigate electric field concentration at the edge of the anode electrode [80]. The field-plated SBDs also showed good on-state device characteristics such as an R_{on} of 5.1 mΩcm^2 and an ideality factor of 1.03. Another edge-termination structure often employed for power SBDs is a guard ring. Our latest SBDs with both a field plate and a N-implanted guard ring, which is schematically illustrated in Fig. 8, achieved an enhancement of V_{br} to 1.43 kV with keeping the same level of R_{on} [81]. Mg-ion implantation doping and fluorine treatment were also employed to form guard rings [82, 83].

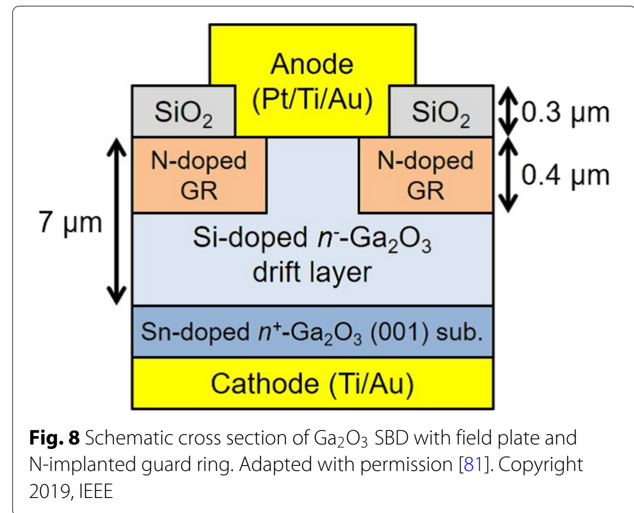

Fig. 8 Schematic cross section of Ga_2O_3 SBD with field plate and N-implanted guard ring. Adapted with permission [81]. Copyright 2019, IEEE

As another attempt to increase V_{br}, β-Ga_2O_3 trench SBDs have also been developed [84–86]. An anode electrode was formed to cover trench sidewalls on which an Al_2O_3 dielectric was deposited. At the reverse-bias condition, the depletion region laterally spreads from the sidewalls, leading to an increase in V_{br}. A very high V_{br} of over 2 kV was demonstrated for the trench SBDs with keeping a low R_{on} of ∼10 mΩcm^2.

7 FET

7.1 Lateral FET

7.1.1 MESFET

The first demonstration of single-crystal Ga_2O_3 transistors was achieved in the form of metal-semiconductor FET (MESFET) as shown in Fig. 9, which was fabricated using a 300-nm-thick Sn-doped n-Ga_2O_3 channel layer grown on a Mg-doped semi-insulating β-Ga_2O_3 (010) substrate by MBE [3]. The MESFET met a basic standard

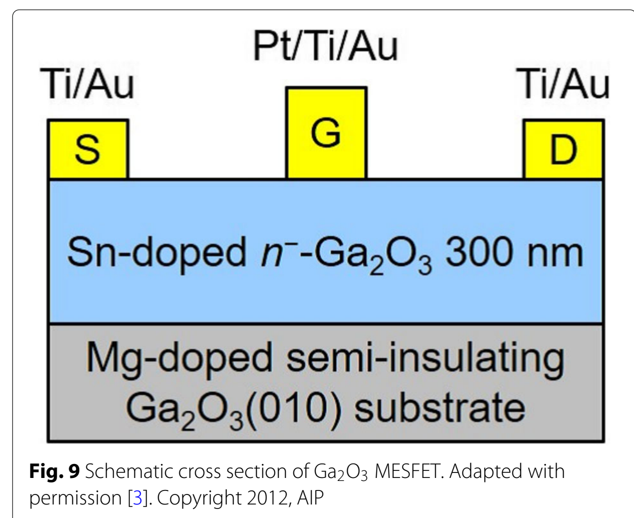

Fig. 9 Schematic cross section of Ga_2O_3 MESFET. Adapted with permission [3]. Copyright 2012, AIP

required as a transistor: drain current (I_d) modulation from the on-state to the off-state by gate voltage (V_g) swing. Although it was the first experimental attempt on fabricating Ga_2O_3 FETs, fundamental device characteristics were reasonably good, such as a maximum I_d of 15 mA/mm at a drain voltage (V_d) of 40 V, a large three-terminal off-state V_{br} of ~250 V, and a high I_d on/off ratio of over four orders of magnitude. However, two shortcomings of poor source/drain ohmic contacts and small surface leakage were noted for the MESFET.

7.1.2 Depletion-mode MOSFET

To improve the ohmic contact, the Si-ion implantation doping process was developed [52], as described in Sections 5.1.1 and 5.2.2. As a next step of β-Ga_2O_3 FET development, we fabricated depletion-mode (D-mode) MOSFETs with Si-implanted n-Ga_2O_3 channel and n^+-Ga_2O_3 ohmic regions, and an Al_2O_3 gate dielectric formed by plasma-assisted atomic layer deposition (ALD), as illustrated in Fig. 10 [87]. Thanks to a large reduction in the ohmic contact resistance, the maximum I_d was largely increased to 65 mA/mm. The gate dielectric contributed to increasing the off-state V_{br} to ~400 V and drastically suppressing an off-state leakage current, which led to a large increase in the I_d on/off ratio to over 10^{10}.

7.1.3 Field-plated MOSFET

Based on the D-mode MOSFETs, β-Ga_2O_3 field-plated MOSFETs were fabricated to further enhance V_{br} by preventing electric field concentration at the drain-side edge portion of the gate metal. Figure 11 shows a cross-sectional schematic of the Ga_2O_3 MOSFET structure with a gate-connected field plate [88]. The field plate successfully contributed to a large enhancement of V_{br} to ~750 V without any degradation of on-state device characteristics from those of the D-mode MOSFETs. The field-plated MOSFETs also exhibited no DC–RF dispersion by virtue of the effect of the thick SiO_2 passivation and high operation stability up to 300°C. Due to the continued development, the V_{br} of lateral β-Ga_2O_3 field-plated MOSFETs has increased to over 2 kV [89, 90].

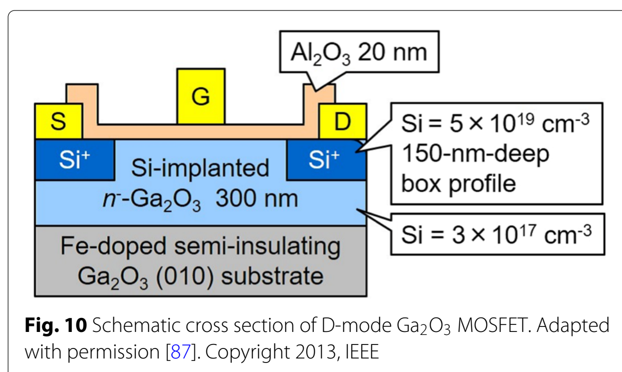

Fig. 10 Schematic cross section of D-mode Ga_2O_3 MOSFET. Adapted with permission [87]. Copyright 2013, IEEE

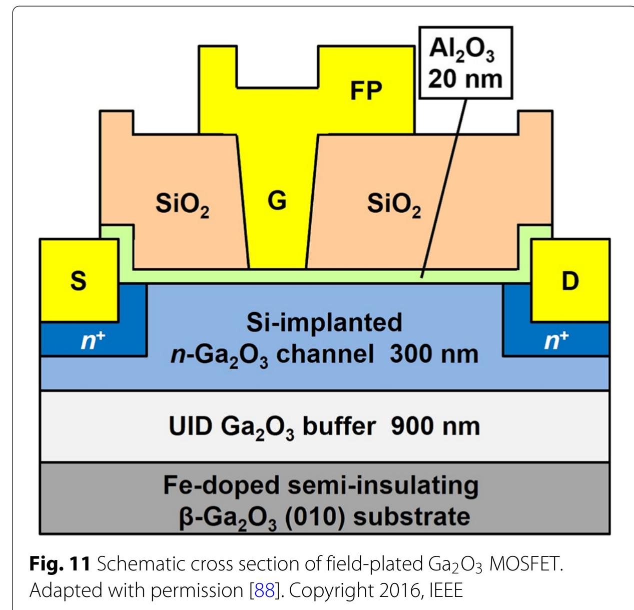

Fig. 11 Schematic cross section of field-plated Ga_2O_3 MOSFET. Adapted with permission [88]. Copyright 2016, IEEE

From the material properties typified by the large E_g, β-Ga_2O_3 is expected to have high resistance against stresses caused by high temperature, radiation, and corrosive gases, as well as being suited for power devices. Hence, it can be considered that β-Ga_2O_3 FETs have a large potential even for wireless communications and signal processing circuits in harsh environments in which it is difficult for existing semiconductor devices to keep operating for a long term. Based on the idea, we also investigated gamma-ray tolerance of the Ga_2O_3 field-plated MOSFETs [91]. The MOSFETs showed only small degradation of DC I_d–V_d output characteristics even after high-dose cumulative gamma-ray irradiation up to 1.6 MGy. Note that the irradiation dose is at a level of exceeding requirements for typical space applications. These results indicate a great potential of β-Ga_2O_3 FETs for applications to high-temperature and/or radiation-hard electronics.

7.1.4 Normally-off MOSFET

Enhancement-mode (E-mode) β-Ga_2O_3 MOSFETs realizing normally-off operation were fabricated by decreasing a thickness and/or a doping concentration of a channel layer to enable full channel depletion under a gate at V_g = 0 V [92]. β-Ga_2O_3 MOSFETs having an unintentionally N-doped Ga_2O_3 channel layer grown by plasma-assisted MBE as illustrated in Fig. 12 demonstrated normally-off operation with a large turn-on threshold V_g of over +8 V [93]. The channel layer with UID N and Si densities of respectively 1×10^{18} and 2×10^{17} cm^{-3} is equivalent to p-type, since deep-acceptor N impurities compensate donor Si ones. These results would imply formation of an

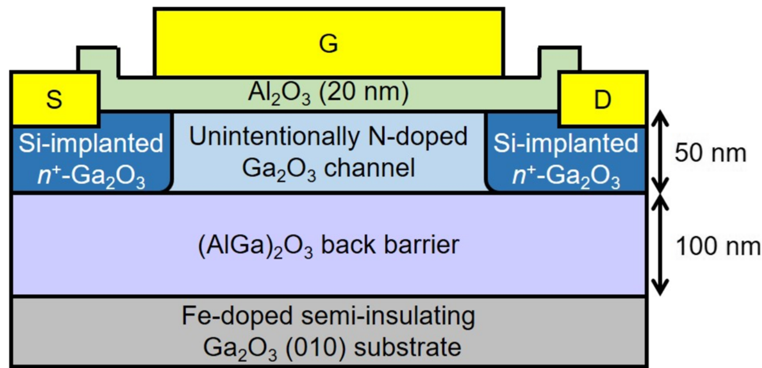

Fig. 12 Schematic cross section of Ga_2O_3 MOSFET with unintentionally N-doped channel. Adapted with permission [93]. Copyright 2019, IEEE

inversion channel at the interface between the Al_2O_3 gate dielectric and the N-doped Ga_2O_3 layer.

7.1.5 *High-frequency MOSFET*

The author's group fabricated highly scaled β-Ga_2O_3 MOSFETs as shown in Fig. 13, which aimed for applications to high-frequency wireless communications and logic circuits operating in harsh environments [94]. The MOSFETs with a gate length (L_g) of 200 nm demonstrated a current-gain cutoff frequency (f_T) of 9 GHz and a maximum oscillation frequency (f_{max}) of 27 GHz. Note that comparable RF small-signal characteristics were also reported from other institutes [95, 96]. These RF device characteristics indicate that β-Ga_2O_3 FETs can be used for wireless communications at frequencies up to $\sim$10 GHz.

7.2 Vertical FET

As of the time of this writing, there have been a few groups developing vertical β-Ga_2O_3 FETs in the world. Two representative developments are discussed in this subsection.

7.2.1 *Current-aperture FET*

Vertical FETs with a current aperture were often selected as a first target in the history of vertical transistor developments due to its simple structure. Figure 14 shows a schematic cross section of a vertical D-mode β-Ga_2O_3 MOSFET with a current aperture that is bounded laterally by N-implanted CBLs [97]. It should be noted that three ion implantation processes were conducted to form the N-doped p-Ga_2O_3 CBLs, a Si-doped n-Ga_2O_3 channel, and heavily Si-doped n^{++}-Ga_2O_3 source ohmic contact regions. Decent device characteristics such as a maximum I_d of 0.42 kA/cm^2 and a specific R_{on} of 31.5 mΩcm^2 were demonstrated. The I_d on/off ratio of over 10^8 was recorded. The three-terminal off-state V_{br} was limited to less than 30 V owing to large electric field in the Al_2O_3 gate dielectric due to the high Si doping density of the channel.

E-mode operation of vertical β-Ga_2O_3 MOSFETs was also demonstrated [98]. The device fabrication process and structure of the E-mode MOSFETs were almost the same as those of the D-mode MOSFETs. There were two modifications from the D-mode structure: a decrease in Si

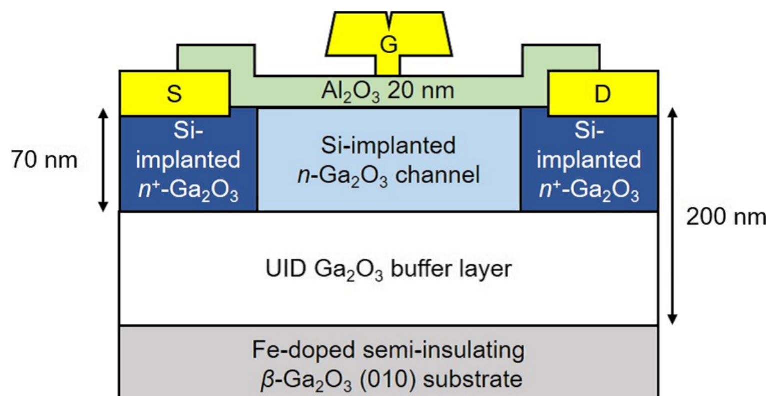

Fig. 13 Schematic cross section of short-gate Ga_2O_3 MOSFET. Adapted with permission [94]. Copyright 2020, AIP

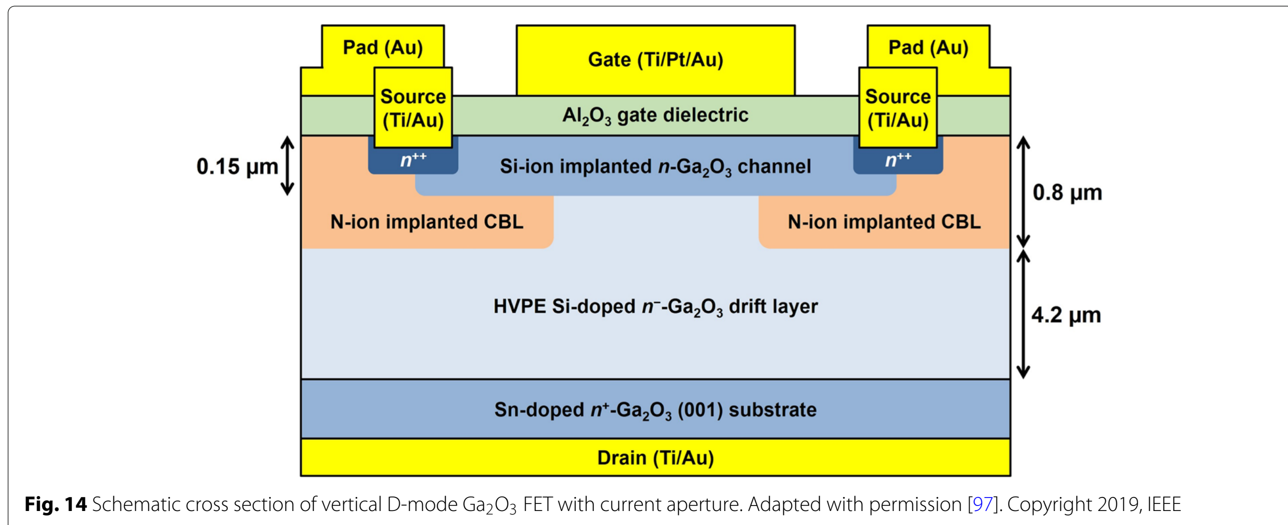

Fig. 14 Schematic cross section of vertical D-mode Ga_2O_3 FET with current aperture. Adapted with permission [97]. Copyright 2019, IEEE

doping density of the channel from 1.5×10^{18} to 5.0×10^{17} cm^{-3} and formation of an n^{++}-region-gate overlap to avoid channel depletion in the gate-source access region at thermal equilibrium. A turn-on threshold V_g of larger than +3 V and an I_d on/off ratio of over 10^6 were attained. The off-state V_{br} was enhanced to ~250 V thanks to the reduction in the Si doping density in the channel.

7.2.2 Fin-channel FET

Top- and side-gate configuration formed on mesa trenches of fin-channel FETs allows superior gate controllability compared with that of planar FETs. The fin-channel FET structures are often developed for low-voltage, high-speed applications; however, the gate configuration is also effective for vertical power FETs on electric-field management. The same group of Cornell University that developed the trench SBDs reported vertical β-Ga_2O_3 FETs with a sub-μm fin channel [99]. E-mode operation was achieved for the devices by means of full channel depletion from the sidewalls at V_g = 0 V. The fin-channel FETs demonstrated excellent device characteristics such as a large I_d of 1 kA/cm^2, a specific R_{on} of 10–20 m$\Omega$$cm^2$, an I_d on/off ratio of ~10^8, and an off-state V_{br} of ~1 kV.

8 Conclusions

This article presents an overview of current R&D status of β-Ga_2O_3 science and engineering, which covers material properties, melt bulk growth, epitaxial thin-film growth, device processing, and state-of-the-art device technologies. The extremely large BFOM and the availability of high-quality, large-diameter single-crystal wafers produced from melt-grown bulks are especially attractive from practical application perspectives. Over the past 10 years, all the aspects of β-Ga_2O_3 material and device technologies have significantly progressed, and several development milestones on the way to industrialization and commercialization of β-Ga_2O_3 FETs and SBDs have already been achieved. It is gratifying that Ga_2O_3 has gained a lot of popularity for the last 10 years thanks to the accomplishments and is now largely accepted as one of the promising UWBG materials in the semiconductor community. However, there is no room for doubt that the current β-Ga_2O_3 device technologies are still immature, and that we still have a long way to start to introduce them into markets. Future intense efforts are indispensable to develop advanced device structures to improve their characteristics. Overcoming the two shortcomings related to fundamental material properties, which are the absence of hole-conductive p-Ga_2O_3 and the poor thermal conductivity, should be tough challenges. The potential of β-Ga_2O_3 devices is worth putting the effort into the developments, because it can be expected that β-Ga_2O_3 power and harsh-environment devices will contribute to global energy saving and creation of new application fields of semiconductor device electronics, respectively. The continued efforts on material and device engineering should lead to generating far-reaching technological and socioeconomic impacts.

Acknowledgements
The author would like to express the deepest appreciation to co-workers and external collaborators for their tremendous contributions in the presented R&D.

Authors' contributions
The author read and approved the final manuscript.

Funding
Part of the work presented in this article was supported by Council for Science, Technology and Innovation (CSTI), Cross-ministerial Strategic Innovation Promotion Program (SIP), Next generation power electronics (funding agency: New Energy and Industrial Technology Development Organization), and the Strategic Information and Communications R&D Promotion Program (SCOPE) of the Ministry of Internal Affairs and Communications, Japan.

Availability of data and materials
All data and materials presented in this article are included in published articles listed in References.

Declarations

Ethics approval and consent to participate
Not applicable.

Consent for publication
Not applicable.

Competing interests
The author declares that he has no competing interests.

Received: 14 October 2021 Accepted: 6 December 2021
Published online: 17 January 2022

References

1. J. Y. Tsao, S. Chowdhury, M. A. Hollis, D. Jena, N. M. Johnson, K. A. Jones, R. J. Kaplar, S. Rajan, C. G. V. d. Walle, E. Bellotti, C. L. Chua, R. Collazo, M. E. Coltrin, J. A. Cooper, K. R. Evans, S. Graham, T. A. Grotjohn, E. R. Heller, M. Higashiwaki, M. S. Islam, P. W. Juodawlkis, M. A. Khan, A. D. Koehler, J. H. Leach, U. K. Mishra, R. J. Nemanich, R. C. N. Pilawa-Podgurski, J. B. Shealy, Z. Sitar, M. J. Tadjer, A. F. Witulski, M. Wraback, J. A. Simmons, Ultrawide-bandgap semiconductors: research opportunities and challenges. Adv. Electron. Mater. **4**(1), 1600501 (2018). https://doi.org/10.1002/aelm.201600501
2. R. Roy, V. G. Hill, E. F. Osborn, Polymorphism of Ga_2O_3 and the system Ga_2O_3–H_2O. J. Am. Chem. Soc. **74**(3), 719–722 (1952). https://doi.org/10.1021/ja01123a039
3. M. Higashiwaki, K. Sasaki, A. Kuramata, T. Masui, S. Yamakoshi, Gallium oxide (Ga_2O_3) metal-semiconductor field-effect transistors on single-crystal β-Ga_2O_3 (010) substrates. Appl. Phys. Lett. **100**(1), 013504 (2012). https://doi.org/10.1063/1.3674287
4. S. Geller, Crystal structure of β-Ga_2O_3. J. Chem. Phys. **33**(3), 676–684 (1960). https://doi.org/10.1063/1.1731237
5. H. He, R. Orlando, M. A. Blanco, R. Pandey, E. Amzallag, I. Baraille, M. Rérat, First-principles study of the structural, electronic, and optical properties of Ga_2O_3 in its monoclinic and hexagonal phases. Phys. Rev. B. **74**, 195123 (2006). https://doi.org/10.1103/PhysRevB.74.195123
6. J. B. Varley, J. R. Weber, A. Janotti, C. G. Van de Walle, Oxygen vacancies and donor impurities in β-Ga_2O_3. Appl. Phys. Lett. **97**(14), 142106 (2010). https://doi.org/10.1063/1.3499306
7. H. Peelaers, C. G. Van de Walle, Brillouin zone and band structure of β-Ga_2O_3. Phys. Status Solidi (b). **252**(4), 828–832 (2015). https://doi.org/10.1002/pssb.201451551
8. Y. Zhang, A. Neal, Z. Xia, C. Joishi, J. M. Johnson, Y. Zheng, S. Bajaj, M. Brenner, D. Dorsey, K. Chabak, G. Jessen, J. Hwang, S. Mou, J. P. Heremans, S. Rajan, Demonstration of high mobility and quantum transport in modulation-doped β-$(Al_xGa_{1-x})_2O_3/Ga_2O_3$ heterostructures. Appl. Phys. Lett. **112**(17), 173502 (2018). https://doi.org/10.1063/1.5025704
9. T. Onuma, S. Saito, K. Sasaki, T. Masui, T. Yamaguchi, T. Honda, M. Higashiwaki, Valence band ordering in β-Ga_2O_3 studied by polarized transmittance and reflectance spectroscopy. Jpn. J. Appl. Phys. **54**(11), 112601 (2015). https://doi.org/10.7567/JJAP.54.112601
10. K. Ghosh, U. Singisetti, Impact ionization in β-Ga_2O_3. J. Appl. Phys. **124**(8), 085707 (2018). https://doi.org/10.1063/1.5034120
11. Z. Xia, H. Chandrasekar, W. Moore, C. Wang, A. J. Lee, J. McGlone, N. K. Kalarickal, A. Arehart, S. Ringel, F. Yang, S. Rajan, Metal/$BaTiO_3$/β-Ga_2O_3 dielectric heterojunction diode with 5.7 MV/cm breakdown field. Appl. Phys. Lett. **115**(25), 252104 (2019). https://doi.org/10.1063/1.5130669
12. T. Onuma, S. Saito, K. Sasaki, K. Goto, T. Masui, T. Yamaguchi, T. Honda, A. Kuramata, M. Higashiwaki, Temperature-dependent exciton resonance energies and their correlation with IR-active optical phonon modes in β-Ga_2O_3 single crystals. Appl. Phys. Lett. **108**(10), 101904 (2016). https://doi.org/10.1063/1.4943175
13. K. Ghosh, U. Singisetti, Ab initio calculation of electron–phonon coupling in monoclinic β-Ga_2O_3 crystal. Appl. Phys. Lett. **109**(7), 072102 (2016). https://doi.org/10.1063/1.4961308
14. N. Ma, N. Tanen, A. Verma, Z. Guo, T. Luo, H. G. Xing, D. Jena, Intrinsic electron mobility limits in β-Ga_2O_3. Appl. Phys. Lett. **109**(21), 212101 (2016). https://doi.org/10.1063/1.4968550
15. K. Goto, K. Konishi, H. Murakami, Y. Kumagai, B. Monemar, M. Higashiwaki, A. Kuramata, S. Yamakoshi, Halide vapor phase epitaxy of Si doped β-Ga_2O_3 and its electrical properties. Thin Solid Films. **666**, 182–184 (2018). https://doi.org/10.1016/j.tsf.2018.09.006
16. Z. Feng, A. F. M. Anhar Uddin Bhuiyan, M. R. Karim, H. Zhao, MOCVD homoepitaxy of Si-doped (010) β-Ga_2O_3 thin films with superior transport properties. Appl. Phys. Lett. **114**(25), 250601 (2019). https://doi.org/10.1063/1.5109678
17. Y. Zhang, F. Alema, A. Mauze, O. S. Koksaldi, R. Miller, A. Osinsky, J. S. Speck, MOCVD grown epitaxial β-Ga_2O_3 thin film with an electron mobility of 176 cm^2/V s at room temperature. APL Mater. **7**(2), 022506 (2019). https://doi.org/10.1063/1.5058059
18. F. Alema, Y. Zhang, A. Osinsky, N. Valente, A. Mauze, T. Itoh, J. S. Speck, Low temperature electron mobility exceeding 10^4 cm^2/V s in MOCVD grown β-Ga_2O_3. APL Mater. **7**(12), 121110 (2019). https://doi.org/10.1063/1.5132954
19. K. Ghosh, U. Singisetti, *Ab initio* velocity-field curves in monoclinic β-Ga_2O_3. J. Appl. Phys. **122**(3), 035702 (2017). https://doi.org/10.1063/1.4986174
20. T. Oishi, K. Harada, Y. Koga, M. Kasu, Conduction mechanism in highly doped β-Ga_2O_3 ($\bar{2}01$) single crystals grown by edge-defined film-fed growth method and their Schottky barrier diodes. Jpn. J. Appl. Phys. **55**(3), 030305 (2016). https://doi.org/10.7567/jjap.55.030305
21. A. T. Neal, S. Mou, S. Rafique, H. Zhao, E. Ahmadi, J. S. Speck, K. T. Stevens, J. D. Blevins, D. B. Thomson, N. Moser, K. D. Chabak, G. H. Jessen, Donors and deep acceptors in β-Ga_2O_3. Appl. Phys. Lett. **113**(6), 062101 (2018). https://doi.org/10.1063/1.5034474
22. J. L. Lyons, A survey of acceptor dopants for β-Ga_2O_3. Semicond. Sci. Technol. **33**(5), 05–02 (2018). https://doi.org/10.1088/1361-6641/aaba98
23. H. Peelaers, J. L. Lyons, J. B. Varley, C. G. Van de Walle, Deep acceptors and their diffusion in Ga_2O_3. APL Mater. **7**(2), 022519 (2019). https://doi.org/10.1063/1.5063807
24. J. B. Varley, A. Janotti, C. Franchini, C. G. Van de Walle, Role of self-trapping in luminescence and p-type conductivity of wide-band-gap oxides. Phys. Rev. B. **85**(8), 081109 (2012). https://doi.org/10.1103/PhysRevB.85.081109
25. P. Deak, Q. Duy Ho, F. Seemann, B. Aradi, M. Lorke, T. Frauenheim, Choosing the correct hybrid for defect calculations: a case study on intrinsic carrier trapping in β-Ga_2O_3. Phys. Rev. B. **95**(7), 075208 (2017). https://doi.org/10.1103/PhysRevB.95.075208
26. T. Gake, Y. Kumagai, F. Oba, First-principles study of self-trapped holes and acceptor impurities in Ga_2O_3 polymorphs. Phys. Rev. Mater. **3**(4), 044603 (2019). https://doi.org/10.1103/PhysRevMaterials.3.044603
27. M. Handwerg, R. Mitdank, Z. Galazka, S. F. Fischer, Temperature-dependent thermal conductivity in Mg-doped and undoped β-Ga_2O_3 bulk-crystals. Semicond. Sci. Technol. **30**(2), 024006 (2015). https://doi.org/10.1088/0268-1242/30/2/024006
28. Z. Guo, A. Verma, X. Wu, F. Sun, A. Hickman, T. Masui, A. Kuramata, M. Higashiwaki, D. Jena, T. Luo, Anisotropic thermal conductivity in single crystal β-gallium oxide. Appl. Phys. Lett. **106**(11), 111909 (2015). https://doi.org/10.1063/1.4916078
29. M. Slomski, N. Blumenschein, P. P. Paskov, J. F. Muth, T. Paskova, Anisotropic thermal conductivity of β-Ga_2O_3 at elevated temperatures: effect of Sn and Fe dopants. J. Appl. Phys. **121**(23), 235104 (2017). https://doi.org/10.1063/1.4986478
30. P. Jiang, X. Qian, X. Li, R. Yang, Three-dimensional anisotropic thermal conductivity tensor of single crystalline β-Ga_2O_3. Appl. Phys. Lett. **113**(23), 232105 (2018). https://doi.org/10.1063/1.5054573
31. B. J. Baliga, Semiconductors for high voltage, vertical channel field effect transistors. J. Appl. Phys. **53**(3), 1759–1764 (1982). https://doi.org/10.1063/1.331646
32. B. J. Baliga, Power semiconductor device figure of merit for high-frequency applications. IEEE Electron Device Lett. **10**(10), 455–457 (1989). https://doi.org/10.1109/55.43098
33. E. Johnson, in *1958 IRE International Convention Record*. Physical limitations on frequency and power parameters of transistors, vol. 13, (1965), pp. 27–34. https://doi.org/10.1109/IRECON.1965.1147520
34. E. G. Víllora, K. Shimamura, Y. Yoshikawa, K. Aoki, N. Ichinose, Large-size β-Ga_2O_3 single crystals and wafers. J. Cryst. Growth. **270**(3), 420–426 (2004). https://doi.org/10.1016/j.jcrysgro.2004.06.027

35. A. Kuramata, K. Koshi, S. Watanabe, Y. Yamaoka, T. Masui, S. Yamakoshi, High-quality β-Ga_2O_3 single crystals grown by edge-defined film-fed growth. Jpn. J. Appl. Phys. **55**(12), 1202–2 (2016). https://doi.org/10.7567/JJAP.55.1202A2
36. Z. Galazka, R. Uecker, D. Klimm, K. Irmscher, M. Naumann, M. Pietsch, A. Kwasniewski, R. Bertram, S. Ganschow, M. Bickermann, Scaling-up of bulk β-Ga_2O_3 single crystals by the Czochralski method. ECS J. Solid State Sci. Technol. **6**(2), 3007 (2016). https://doi.org/10.1149/2.0021702jss
37. J. D. Blevins, K. Stevens, A. Lindsey, G. Foundos, L. Sande, Development of large diameter semi-insulating gallium oxide (Ga_2O_3) substrates. IEEE Trans. Semicond. Manuf. **32**(4), 466–472 (2019). https://doi.org/10.1109/TSM.2019.2944526
38. K. Hoshikawa, T. Kobayashi, E. Ohba, T. Kobayashi, 50 mm diameter Sn-doped (001) β-Ga_2O_3 crystal growth using the vertical Bridgeman technique in ambient air. J. Cryst. Growth. **546**, 125778 (2020). https://doi.org/10.1016/j.jcrysgro.2020.125778
39. H. Aida, K. Nishiguchi, H. Takeda, N. Aota, K. Sunakawa, Y. Yaguchi, Growth of β-Ga_2O_3 single crystals by the edge-defined, film fed growth method. Jpn. J. Appl. Phys. **47**(11R), 8506 (2008). https://doi.org/10.1143/JJAP.47.8506
40. P. Vogt, O. Bierwagen, Reaction kinetics and growth window for plasma-assisted molecular beam epitaxy of Ga_2O_3: incorporation of Ga vs. Ga_2O desorption. Appl. Phys. Lett. **108**(7), 072101 (2016). https://doi.org/10.1063/1.4942002
41. K. Sasaki, A. Kuramata, T. Masui, E. G. Villora, K. Shimamura, S. Yamakoshi, Device-quality β-Ga_2O_3 epitaxial films fabricated by ozone molecular beam epitaxy. Appl. Phys. Express. **5**(3), 035502 (2012). https://doi.org/10.1143/APEX.5.035502
42. E. Ahmadi, O. S. Koksaldi, S. W. Kaun, Y. Oshima, D. B. Short, U. K. Mishra, J. S. Speck, Ge doping of β-Ga_2O_3 films grown by plasma-assisted molecular beam epitaxy. Appl. Phys. Express. **10**(4), 041102 (2017). https://doi.org/10.7567/APEX.10.041102
43. N. K. Kalarickal, Z. Xia, J. McGlone, S. Krishnamoorthy, W. Moore, M. Brenner, A. R. Arehart, S. A. Ringel, S. Rajan, Mechanism of Si doping in plasma assisted MBE growth of β-Ga_2O_3. Appl. Phys. Lett. **115**(15), 152106 (2019). https://doi.org/10.1063/1.5123149
44. A. Mauze, Y. Zhang, T. Itoh, E. Ahmadi, J. S. Speck, Sn doping of (010) β-Ga_2O_3 films grown by plasma-assisted molecular beam epitaxy. Appl. Phys. Lett. **117**(22), 222102 (2020). https://doi.org/10.1063/5.0027870
45. K. Sasaki, M. Higashiwaki, A. Kuramata, T. Masui, S. Yamakoshi, Growth temperature dependences of structural and electrical properties of Ga_2O_3 epitaxial films grown on β-Ga_2O_3 (010) substrates by molecular beam epitaxy. J. Cryst. Growth. **392**, 30–33 (2014). https://doi.org/10.1016/j.jcrysgro.2014.02.002
46. K. Nomura, K. Goto, R. Togashi, H. Murakami, Y. Kumagai, A. Kuramata, S. Yamakoshi, A. Koukitu, Thermodynamic study of β-Ga_2O_3 growth by halide vapor phase epitaxy. J. Cryst. Growth. **405**, 19–22 (2014). https://doi.org/10.1016/j.jcrysgro.2014.06.051
47. H. Murakami, K. Nomura, K. Goto, K. Sasaki, K. Kawara, Q. T. Thieu, R. Togashi, Y. Kumagai, M. Higashiwaki, A. Kuramata, S. Yamakoshi, B. Monemar, A. Koukitu, Homoepitaxial growth of β-Ga_2O_3 layers by halide vapor phase epitaxy. Appl. Phys. Express. **8**(1), 015503 (2014). https://doi.org/10.7567/APEX.8.015503
48. M. J. Tadjer, F. Alema, A. Osinsky, M. A. Mastro, N. Nepal, J. M. Woodward, R. L. Myers-Ward, E. R. Glaser, J. A. Freitas, A. G. Jacobs, J. C. Gallagher, A. L. Mock, D. J. Pennachio, J. Hajzus, M. Ebrish, T. J. Anderson, K. D. Hobart, J. K. Hite, C. R. E. Jr, Characterization of β-Ga_2O_3 homoepitaxial films and MOSFETs grown by MOCVD at high growth rates. J. Phys. D Appl. Phys. **54**(3), 034005 (2021). https://doi.org/10.1088/1361-6463/abbc96
49. F. Alema, Y. Zhang, A. Osinsky, N. Orishchin, N. Valente, A. Mauze, J. S. Speck, Low 10^{14} cm?3 free carrier concentration in epitaxial β-Ga_2O_3 grown by MOCVD. APL Mater. **8**(2), 021110 (2020). https://doi.org/10.1063/1.5132752
50. A. F. M. Anhar Uddin Bhuiyan, Z. Feng, J. M. Johnson, Z. Chen, H.-L. Huang, J. Hwang, H. Zhao, MOCVD epitaxy of β-$(Al_xGa_{1-x})_2O_3$ thin films on (010) Ga_2O_3 substrates and N-type doping. Appl. Phys. Lett. **115**(12), 120602 (2019). https://doi.org/10.1063/1.5123495
51. P. Ranga, A. Bhattacharyya, A. Rishinaramangalam, Y. K. Ooi, M. A. Scarpulla, D. Feezell, S. Krishnamoorthy, Delta-doped β-Ga_2O_3 thin films and β-$(Al_{0.26}Ga_{0.74})_2O_3$/$\beta$-$Ga_2O_3$ heterostructures grown by metalorganic vapor-phase epitaxy. Appl. Phys. Express. **13**(4), 045501 (2020). https://doi.org/10.35848/1882-0786/ab7712
52. K. Sasaki, M. Higashiwaki, A. Kuramata, T. Masui, S. Yamakoshi, Si-ion implantation doping in β-Ga_2O_3 and its application to fabrication of low-resistance ohmic contacts. Appl. Phys. Express. **6**(8), 086502 (2013). https://doi.org/10.7567/APEX.6.086502
53. M. H. Wong, K. Sasaki, A. Kuramata, S. Yamakoshi, M. Higashiwaki, Electron channel mobility in silicon-doped Ga_2O_3 MOSFETs with a resistive buffer layer. Jpn. J. Appl. Phys. **55**(12), 1202–9 (2016). https://doi.org/10.7567/JJAP.55.1202B9
54. M. H. Wong, C.-H. Lin, A. Kuramata, S. Yamakoshi, H. Murakami, Y. Kumagai, M. Higashiwaki, Acceptor doping of β-Ga_2O_3 by Mg and N ion implantations. Appl. Phys. Lett. **113**(10), 102103 (2018). https://doi.org/10.1063/1.5050040
55. Y. Yao, R. Gangireddy, J. Kim, K. K. Das, R. F. Davis, L. M. Porter, Electrical behavior of β-Ga_2O_3 Schottky diodes with different Schottky metals. J. Vac. Sci. Technol. B. **35**(3), 03–113 (2017). https://doi.org/10.1116/1.4980042
56. E. Farzana, Z. Zhang, P. K. Paul, A. R. Arehart, S. A. Ringel, Influence of metal choice on (010) β-Ga_2O_3 Schottky diode properties. Appl. Phys. Lett. **110**(20), 202102 (2017). https://doi.org/10.1063/1.4983610
57. L. A. M. Lyle, K. Jiang, E. V. Favela, K. Das, A. Popp, Z. Galazka, G. Wagner, L. M. Porter, Effect of metal contacts on (100) β-Ga_2O_3 Schottky barriers. J. Vacuum Sci. Technol. A. **39**(3), 033202 (2021). https://doi.org/10.1116/6.0000877
58. T. Harada, A. Tsukazaki, Control of Schottky barrier height in metal/β-Ga_2O_3 junctions by insertion of $PdCoO_2$ layers. APL Mater. **8**(4), 041109 (2020). https://doi.org/10.1063/1.5145117
59. Z. Xia, C. Joishi, S. Krishnamoorthy, S. Bajaj, Y. Zhang, M. Brenner, S. Lodha, S. Rajan, Delta doped β-Ga_2O_3 field effect transistors with regrown ohmic contacts. IEEE Electron Device Lett. **39**(4), 568–571 (2018). https://doi.org/10.1109/LED.2018.2805785
60. A. Bhattacharyya, S. Roy, P. Ranga, D. Shoemaker, Y. Song, J. S. Lundh, S. Choi, S. Krishnamoorthy, 130 mA mm^{-1} β-Ga_2O_3 metal semiconductor field effect transistor with low-temperature metalorganic vapor phase epitaxy-regrown ohmic contacts. Appl. Phys. Express. **14**(7), 076502 (2021). https://doi.org/10.35848/1882-0786/ac07ef
61. M.-H. Lee, R. L. Peterson, Interfacial reactions of titanium/gold ohmic contacts with Sn-doped β-Ga_2O_3. APL Mater. **7**(2), 022524 (2019). https://doi.org/10.1063/1.5054624
62. M.-H. Lee, R. L. Peterson, Accelerated aging stability of β-Ga_2O_3–titanium/gold ohmic interfaces. ACS Appl. Mater. Interfaces. **12**(41), 46277–46287 (2020). https://doi.org/10.1021/acsami.0c10598
63. L. A. M. Lyle, T. C. Back, C. T. Bowers, A. J. Green, K. D. Chabak, D. L. Dorsey, E. R. Heller, L. M. Porter, Electrical and chemical analysis of Ti/Au contacts to β-Ga_2O_3. APL Mater. **9**(6), 061104 (2021). https://doi.org/10.1063/5.0051340
64. T. Oshima, R. Wakabayashi, M. Hattori, A. Hashiguchi, N. Kawano, K. Sasaki, T. Masui, A. Kuramata, S. Yamakoshi, K. Yoshimatsu, A. Ohtomo, T. Oishi, M. Kasu, Formation of indium-tin oxide ohmic contacts for β-Ga_2O_3. Jpn. J. Appl. Phys. **55**(12), 1202–7 (2016). https://doi.org/10.7567/JJAP.55.1202B7
65. P. H. Carey, J. Yang, F. Ren, D. C. Hays, S. J. Pearton, S. Jang, A. Kuramata, I. I. Kravchenko, Ohmic contacts on n-type β-Ga_2O_3 using AZO/Ti/Au. AIP Adv. **7**(9), 095313 (2017). https://doi.org/10.1063/1.4996172
66. P. H. Carey, J. Yang, F. Ren, D. C. Hays, S. J. Pearton, A. Kuramata, I. I. Kravchenko, Improvement of ohmic contacts on Ga_2O_3 through use of ITO-interlayers. J. Vac. Sci. Technol. B. **35**(6), 061201 (2017). https://doi.org/10.1116/1.4995816
67. J. E. Hogan, S. W. Kaun, E. Ahmadi, Y. Oshima, J. S. Speck, Chlorine-based dry etching of β-Ga_2O_3. Semicond. Sci. Technol. **31**(6), 065006 (2016). https://doi.org/10.1088/0268-1242/31/6/065006
68. L. Zhang, A. Verma, H. G. Xing, D. Jena, Inductively-coupled-plasma reactive ion etching of single-crystal β-Ga_2O_3. Jpn. J. Appl. Phys. **56**(3), 030304 (2017). https://doi.org/10.7567/JJAP.56.030304
69. T. Oshima, T. Okuno, N. Arai, Y. Kobayashi, S. Fujita, Wet etching of β-Ga_2O_3 substrates. Jpn. J. Appl. Phys. **48**(4R), 040208 (2009). https://doi.org/10.1143/JJAP.48.040208
70. Y. Zhang, A. Mauze, J. S. Speck, Anisotropic etching of β-Ga_2O_3 using hot phosphoric acid. Appl. Phys. Lett. **115**(1), 013501 (2019). https://doi.org/10.1063/1.5093188

71. G. Alfieri, A. Mihaila, P. Godignon, J. B. Varley, L. Vines, Deep level study of chlorine-based dry etched β-Ga_2O_3. J. Appl. Phys. **130**(2), 025701 (2021). https://doi.org/10.1063/5.0050416
72. Y. Zhang, A. Mauze, F. Alema, A. Osinsky, J. S. Speck, Near unity ideality factor for sidewall Schottky contacts on un-intentionally doped β-Ga_2O_3. Appl. Phys. Express. **12**(4), 044005 (2019). https://doi.org/10.7567/1882-0786/ab08ad
73. H.-C. Huang, M. Kim, X. Zhan, K. Chabak, J. D. Kim, A. Kvit, D. Liu, Z. Ma, J.-M. Zuo, X. Li, High aspect ratio β-Ga_2O_3 fin arrays with low-interface charge density by inverse metal-assisted chemical etching. ACS Nano. **13**(8), 8784–8792 (2019). https://doi.org/10.1021/acsnano.9b01709
74. C.-H. Lin, N. Hatta, K. Konishi, S. Watanabe, A. Kuramata, K. Yagi, M. Higashiwaki, Single-crystal-Ga_2O_3/polycrystalline-SiC bonded substrate with low thermal and electrical resistances at the heterointerface. Appl. Phys. Lett. **114**(3), 032103 (2019). https://doi.org/10.1063/1.5051720
75. T. Matsumae, Y. Kurashima, H. Umezawa, K. Tanaka, T. Ito, H. Watanabe, H. Takagi, Low-temperature direct bonding of β-Ga_2O_3 and diamond substrates under atmospheric conditions. Appl. Phys. Lett. **116**(14), 141602 (2020). https://doi.org/10.1063/5.0002068
76. T. Matsumae, Y. Kurashima, H. Takagi, H. Umezawa, E. Higurashi, Low-temperature direct bonding of SiC and Ga_2O_3 substrates under atmospheric conditions. J. Appl. Phys. **130**(8), 085303 (2021). https://doi.org/10.1063/5.0057960
77. Y. Song, D. Shoemaker, J. H. Leach, C. McGray, H.-L. Huang, A. Bhattacharyya, Y. Zhang, C. U. Gonzalez-Valle, T. Hess, S. Zhukovsky, K. Ferri, R. M. Lavelle, C. Perez, D. W. Snyder, J.-P. Maria, B. Ramos-Alvarado, X. Wang, S. Krishnamoorthy, J. Hwang, B. M. Foley, S. Choi, Ga_2O_3-on-sic composite wafer for thermal management of ultrawide bandgap electronics. ACS Appl. Mater. Interfaces. **13**(34), 40817–40829 (2021). https://doi.org/10.1021/acsami.1c09736
78. K. Sasaki, M. Higashiwaki, A. Kuramata, T. Masui, S. Yamakoshi, Ga_2O_3 Schottky barrier diodes fabricated by using single-crystal β-Ga_2O_3 (010) substrates. IEEE Electron Device Lett. **34**(4), 493–495 (2013). https://doi.org/10.1109/LED.2013.2244057
79. M. Higashiwaki, K. Konishi, K. Sasaki, K. Goto, K. Nomura, Q. T. Thieu, R. Togashi, H. Murakami, Y. Kumagai, B. Monemar, A. Koukitu, A. Kuramata, S. Yamakoshi, Temperature-dependent capacitance–voltage and current–voltage characteristics of Pt/Ga_2O_3 (001) Schottky barrier diodes fabricated on n^--Ga_2O_3 drift layers grown by halide vapor phase epitaxy. Appl. Phys. Lett. **108**(13), 133503 (2016). https://doi.org/10.1063/1.4945267
80. K. Konishi, K. Goto, H. Murakami, Y. Kumagai, A. Kuramata, S. Yamakoshi, M. Higashiwaki, 1-kV vertical Ga_2O_3 field-plated Schottky barrier diodes. Appl. Phys. Lett. **110**(10), 103506 (2017). https://doi.org/10.1063/1.4977857
81. C.-H. Lin, Y. Yuda, M. H. Wong, M. Sato, N. Takekawa, K. Konishi, T. Watahiki, M. Yamamuka, H. Murakami, Y. Kumagai, M. Higashiwaki, Vertical Ga_2O_3 Schottky barrier diodes with guard ring formed by nitrogen-ion implantation. IEEE Electron Device Lett. **40**(9), 1487–1490 (2019). https://doi.org/10.1109/LED.2019.2927790
82. H. Zhou, Q. Yan, J. Zhang, Y. Lv, Z. Liu, Y. Zhang, K. Dang, P. Dong, Z. Feng, Q. Feng, J. Ning, C. Zhang, P. Ma, Y. Hao, High-performance vertical β-Ga_2O_3 Schottky barrier diode with implanted edge termination. IEEE Electron Device Lett. **40**(11), 1788–1791 (2019). https://doi.org/10.1109/LED.2019.2939788
83. Z. Hu, Y. Lv, C. Zhao, Q. Feng, Z. Feng, K. Dang, X. Tian, Y. Zhang, J. Ning, H. Zhou, X. Kang, J. Zhang, Y. Hao, Beveled fluoride plasma treatment for vertical β-Ga_2O_3 Schottky barrier diode with high reverse blocking voltage and low turn-on voltage. IEEE Electron Device Lett. **41**(3), 441–444 (2020). https://doi.org/10.1109/LED.2020.2968587
84. W. Li, K. Nomoto, Z. Hu, D. Jena, H. G. Xing, Fin-channel orientation dependence of forward conduction in kV-class Ga_2O_3 trench Schottky barrier diodes. Appl. Phys. Express. **12**(6), 061007 (2019). https://doi.org/10.7567/1882-0786/ab206c
85. W. Li, K. Nomoto, Z. Hu, D. Jena, H. G. Xing, Guiding principles for trench schottky barrier diodes based on ultrawide bandgap semiconductors: a case study in Ga_2O_3. IEEE Trans. Electron Devices. **67**(10), 3938–3947 (2020). https://doi.org/10.1109/TED.2020.3003292
86. W. Li, K. Nomoto, Z. Hu, D. Jena, H. G. Xing, On-resistance of Ga_2O_3 trench-MOS Schottky barrier diodes: role of sidewall interface trapping. IEEE Trans. Electron Devices. **68**(5), 2420–2426 (2021). https://doi.org/10.1109/TED.2021.3067856
87. M. Higashiwaki, K. Sasaki, M. H. Wong, T. Kamimura, D. Krishnamurthy, A. Kuramata, T. Masui, S. Yamakoshi, in *2013 IEEE International Electron Devices Meeting*. Depletion-mode Ga_2O_3 MOSFETs on β-Ga_2O_3 (010) substrates with Si-ion-implanted channel and contacts, (2013), pp. 28–712874. https://doi.org/10.1109/IEDM.2013.6724713
88. M. H. Wong, K. Sasaki, A. Kuramata, S. Yamakoshi, M. Higashiwaki, Field-plated Ga_2O_3 MOSFETs with a breakdown voltage of over 750 V. IEEE Electron Device Lett. **37**(2), 212–215 (2016). https://doi.org/10.1109/LED.2015.2512279
89. J. K. Mun, K. Cho, W. Chang, H.-W. Jung, J. Do, 2.32 kV breakdown voltage lateral β-Ga_2O_3 MOSFETs with source-connected field plate. ECS J. Solid State Sci. Technol. **8**(7), 3079–3082 (2019). https://doi.org/10.1149/2.0151907jss
90. Y. Lv, H. Liu, X. Zhou, Y. Wang, X. Song, Y. Cai, Q. Yan, C. Wang, S. Liang, J. Zhang, Z. Feng, H. Zhou, S. Cai, Y. Hao, Lateral β-Ga_2O_3 MOSFETs with high power figure of merit of 277 MW/cm^2. IEEE Electron Device Lett. **41**(4), 537–540 (2020). https://doi.org/10.1109/LED.2020.2974515
91. M. H. Wong, A. Takeyama, T. Makino, T. Ohshima, K. Sasaki, A. Kuramata, S. Yamakoshi, M. Higashiwaki, Radiation hardness of β-Ga_2O_3 metal-oxide-semiconductor field-effect transistors against gamma-ray irradiation. Appl. Phys. Lett. **112**(2), 023503 (2018). https://doi.org/10.1063/1.5017810
92. M. H. Wong, Y. Nakata, A. Kuramata, S. Yamakoshi, M. Higashiwaki, Enhancement-mode Ga_2O_3 MOSFETs with Si-ion-implanted source and drain. Appl. Phys. Express. **10**(4), 041101 (2017). https://doi.org/10.7567/APEX.10.041101
93. T. Kamimura, Y. Nakata, M. H. Wong, M. Higashiwaki, Normally-off Ga_2O_3 MOSFETs with unintentionally nitrogen-doped channel layer grown by plasma-assisted molecular beam epitaxy. IEEE Electron Device Lett. **40**(7), 1064–1067 (2019). https://doi.org/10.1109/LED.2019.2919251
94. T. Kamimura, Y. Nakata, M. Higashiwaki, Delay-time analysis in radio-frequency β-Ga_2O_3 field effect transistors. Appl. Phys. Lett. **117**(25), 253501 (2020). https://doi.org/10.1063/5.0029530
95. K. D. Chabak, D. E. Walker, A. J. Green, A. Crespo, M. Lindquist, K. Leedy, S. Tetlak, R. Gilbert, N. A. Moser, G. Jessen, in *2018 IEEE MTT-S International Microwave Workshop Series on Advanced Materials and Processes for RF and THz Applications (IMWS-AMP)*. Sub-micron gallium oxide radio frequency field-effect transistors, (2018), pp. 1–3. https://doi.org/10.1109/IMWS-AMP.2018.8457153
96. Z. Xia, H. Xue, C. Joishi, J. Mcglone, N. K. Kalarickal, S. H. Sohel, M. Brenner, A. Arehart, S. Ringel, S. Lodha, W. Lu, S. Rajan, β-Ga_2O_3 delta-doped field-effect transistors with current gain cutoff frequency of 27 GHz. IEEE Electron Device Lett. **40**(7), 1052–1055 (2019). https://doi.org/10.1109/LED.2019.2920366
97. M. H. Wong, K. Goto, H. Murakami, Y. Kumagai, M. Higashiwaki, Current aperture vertical β-Ga_2O_3 MOSFETs fabricated by N- and Si-ion implantation doping. IEEE Electron Device Lett. **40**(3), 431–434 (2019). https://doi.org/10.1109/LED.2018.2884542
98. M. H. Wong, H. Murakami, Y. Kumagai, M. Higashiwaki, Enhancement-mode β-Ga_2O_3 current aperture vertical MOSFETs with N-ion-implanted blocker. IEEE Electron Device Lett. **41**(2), 296–299 (2020). https://doi.org/10.1109/LED.2019.2962657
99. W. Li, K. Nomoto, Z. Hu, T. Nakamura, D. Jena, H. G. Xing, in *2019 IEEE International Electron Devices Meeting (IEDM)*. Single and multi-fin normally-off Ga_2O_3 vertical transistors with a breakdown voltage over 2.6 kV, (2019), pp. 12–411244. https://doi.org/10.1109/IEDM19573.2019.8993526

Publisher's Note

Springer Nature remains neutral with regard to jurisdictional claims in published maps and institutional affiliations.